Datasheet for 600-101-215

GFP Antibody

Overview

Description:	Anti-GFP (GOAT) Antibody - 600-101-215
Item No.:	600-101-215
Size:	1 mg
Applications:	ELISA, IF, WB, EM, FC, FISH, IHC, IP, Multiplex, Other, Purification
Reactivity:	GFP, eGFP, rGFP
Host Species:	Goat

Product Details

Background:	Green fluorescent protein is a 27 kDa protein produced from the jellyfish Aequorea victoria, which emits green light (emission peak at a wavelength of 509nm) when excited by blue light. GFP is an important tool in cell biology research. GFP is widely used enabling researchers to visualize and localize GFP-tagged proteins within living cells without the need for chemical staining.
Synonyms:	goat anti-GFP Antibody, GFP, Green Fluorescent Protein, GFP antibody, Green Fluorescent Protein antibody, EGFP, enhanced Green Fluorescent Protein, Aequorea victoria, Jellyfish
Host Species:	Goat
Clonality:	Polyclonal
Format:	IgG

Target Details

Reactivity:	GFP, eGFP, rGFP
Immunogen Type:	Recombinant Protein
Immunogen:	The immunogen is a Green Fluorescent Protein (GFP) fusion protein corresponding to the full length amino acid sequence (246aa) derived from the jellyfish Aequorea victoria.

Purity/Specificity:	GFP antibody was prepared from monospecific antiserum by immunoaffinity chromatography using Green Fluorescent Protein (Aequorea victoria) coupled to agarose beads followed by solid phase adsorption(s) to remove any unwanted reactivities. Assay by immunoelectrophoresis resulted in a single precipitin arc against anti-Goat Serum and purified and partially purified Green Fluorescent Protein (Aequorea victoria). No reaction was observed against Human, Mouse or Rat serum proteins.
Relevant Links:	• 600-101-215 SDS • UniProtKB - P42212

Application Details

Tested Applications:	ELISA, IF, WB
Suggested Applications:	EM, FC, FISH, IHC, IP, Multiplex, Other, Purification (Based on references)
Application Note:	Anti-GFP is designed to detect GFP and its variants. Goat Anti-GFP has been tested by ELISA, Western blot, and immunofluorescence. This product is also suitable for EM, FC, FISH, IHC, IP, purification, and multiplex assays based on published references. This antibody can be used to detect GFP by ELISA (sandwich or capture) for the direct binding of antigen and recognizes wild-type, recombinant, and enhanced forms of GFP. Researchers should determine optimal titers for applications.
Assay Dilutions:	All assays should be optimized by the user. Recommended dilutions (if any) may be listed below.
ELISA:	1:10,000 - 1:30,000
FC:	User Optimized
IF:	1:500
IHC:	1:200 - 1:1,000
IP:	User Optimized
WB:	1:1,000 - 1:10,000
Other:	FISH, Immuno-EM, TEM

Formulation

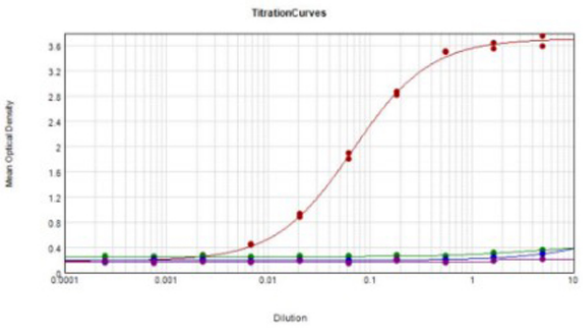
Physical State:	Liquid (sterile filtered)
Concentration:	1.11 mg/mL by UV absorbance at 280 nm
Buffer:	0.02 M Potassium Phosphate, 0.15 M Sodium Chloride, pH 7.2
Preservative:	0.01% (w/v) Sodium Azide

Stabilizer:	None

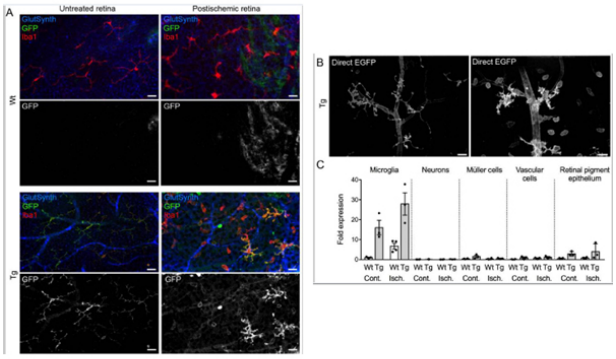
Shipping & Handling

Shipping Condition:	Dry Ice
Storage Condition:	Store GFP antibody at -20° C prior to opening. Aliquot contents and freeze at -20° C or below for extended storage. Avoid cycles of freezing and thawing. Centrifuge product if not completely clear after standing at room temperature. This product is stable for several weeks at 4° C as an undiluted liquid. Dilute only prior to immediate use.
Expiration:	Expiration date is one (1) year from date of receipt.

Images

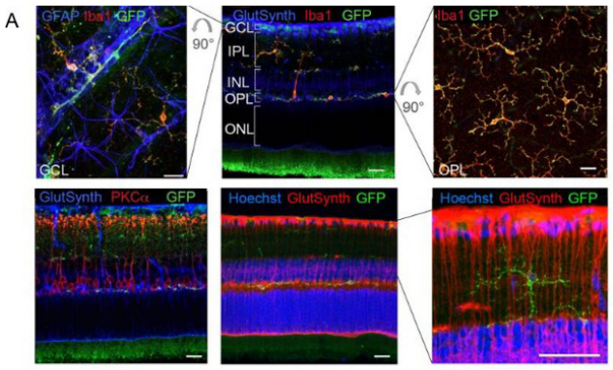


ELISA
ELISA results of purified Goat Anti-GFP Antibody mx3. Each well was coated in 1.0 µg of antigen GFP [Red Line], human IgG [Green Line], Mouse IgG [Blue Line], and Rat IgG [Purple Line]. The starting dilution of antibody was 5 µg/mL and the X-axis represents the Log10 of a 3-fold dilution. The titer is 1:14,800. This titration is a 4-parameter curve fit where the IC50 is defined as the titer of the antibody. Assay performed using Buffer (p/n MB-060-1000), Substrate (p/n TMB-8000), and Donkey Anti-Goat IgG Antibody HRP (p/n 605-703-125).



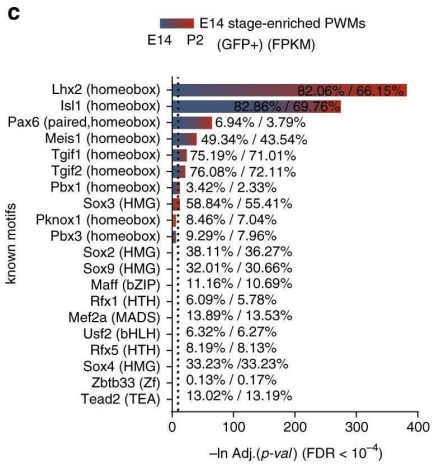
Immunofluorescence Microscopy

Upregulation of P2X7 expression in postischemic retinae 3 days post injury (dpi) of wt and P2X7-EGFP transgenic animals. (A) Retinal flat mount scanned at the plane of the ganglion cell layer (GCL) to delineate microglia residing in this retinal layer. Co-labeling for GFP (600-101-215, Rockland), Iba1 (marker for microglia/macrophages) and glutamine synthetase (marker for Müller glia) shows that EGFP exclusively co-localizes with microglia and in the postischemic retina also with morphologically distinct Iba1-positive cells that likely correspond to infiltrated macrophages. Note unspecific vessel staining caused by the secondary antibody against glutamine synthetase. Scale bars: 20 µm. n = 2 individual line 61 in FVB/C57b/6 hybrid mice. (B) Direct EGFP-fluorescence captured at identical microscope settings in non-fixed retinal flatmounts focused on the GCL shows increased EGFP signal in vessels and microglia and an increase in the number of microglia and/or macrophages. Scale bar: 20 µm. (C) P2X7 expression determined by quantitative real-time PCR on the indicated cell types isolated by immunomagnetic separation from control and postischemic (3 dpi) retinae of line 17 P2X7-EGFP transgenic mice in (C57b/6 background). Bars represent mean ±SEM and include data from 3 to 4 animals/each genotype/condition. Significance between expression level in the untreated control eye of the respective genotype was analyzed using unpaired two-tailed Mann-Whitney-U-test and indicated as: *p<0.05. Data were normalized to the housekeeper pyruvate dehydrogenase beta (PDHB) and results are presented as relative expression levels compared to that in microglia of healthy wild-type retinae. Increase in P2X7 signal in RPE is most likely due to contamination by infiltrating immune cells. Figure provided by CiteAb. Source: Elife, PMID: 30074479.



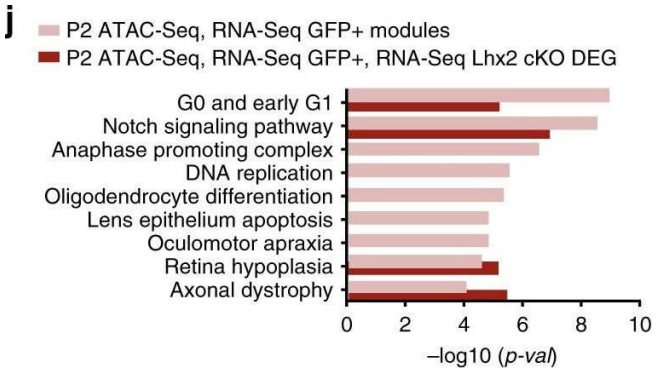
Immunofluorescence Microscopy

P2X7-EGFP expression in retina, sciatic nerves, spinal cord, and at the neuromuscular synapse. (A) EGFP exclusively co-localizes with microglia and endothelial cells in the adult mouse retina. Upper panel: Middle, retinal slice labeled for GFP (600-101-215, Rockland), Iba1 (marker for microglia/macrophages) and glutamine synthetase (marker for Müller glia). Left and right, retinal flat mounts scanned at the plane of the ganlion cell layer (GCL) and outer plexiform layer (OPL), respectively, to delineate microglia residing in these retinal layers. Astrocytes in the GCL were labeled with GFAP. IPL, inner plexiform layer; INL, inner nuclear layer; ONL, outer nuclear layer. Lower panel: Co-staining of EGFP with neuronal marker PKCα (left) and glutamine synthetase (two right panels) at higher contrast and resolution to show absence of neuronal P2X7-EGFP. Cell nuclei were counterstained with Hoechst 33342 (blue) Scale bars: 20 µm. n = 2 individual line 61 in FVB/C57b/6 hybrid mice. Figure provided by CiteAb. Source: Elife, PMID: 30074479.



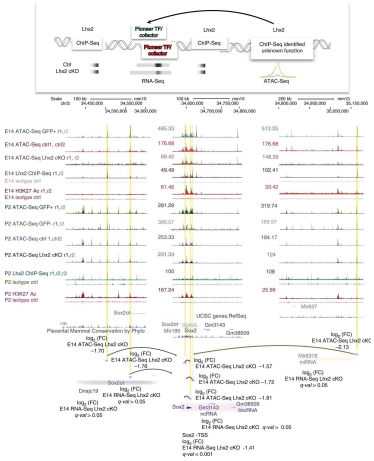
Flow Cytometry

Binding sites for transcription factors with predicted pioneer function co-occur with LHX2 peaks. (a, b) Hierarchical clustering of LHX2 ChIP-Seq regulatory motifs and assigned representative logos are represented at E14 (a) and P2 (b) (linkage = average; similarity threshold cor = 0.6, ncor = 0.4, w = 5). The most enriched cluster comprises LHX2 and multiple variations of the same motif. (c, d) Known transcription factor motifs preferentially enriched in either E14 or P2 LHX2 ChIP-Seq peaks and identified by pairwise comparison are shown. Percentage of motif occurrences are reported for input and background datasets. The relative expression level of the corresponding transcription factor mRNA at E14/P2 is indicated by the blue/red color gradient, respectively Figure provided by CiteAb. Source: Commun Biol, PMID: 31044167.



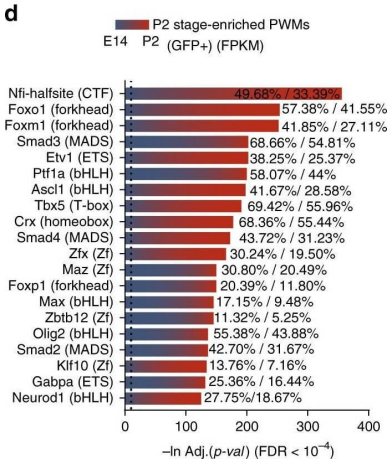
Flow Cytometry

LHX2 regulates cell cycle genes and the Notch signaling pathway by targeting promoters and non-coding elements in nucleosome free regions associated with active enhancers. A) LHX2 motif density around the centers of ChIP-Seq peaks at E14 and P2. B) Enrichment of LHX2 ChIP-Seq peaks distributed across different genomic regions (log2 fold enrichment). (C-F) Percentage of LHX2 target genes in retinal term assigned to at least one age-matched LHX2 ChIP-Seq peak. Enrichment was computed between target genes in term and total number of known genes in term (Supplementary Table 4 and Supplementary Data 1) for peaks shared at E14 and P2 (C), stage-specific peaks (D), and all peaks detected at E14 (E) and P2 (F). RNA-Seq from age-matched Lhx2 cKO retinas identifies Lhx2-dependent genes sets. (*p-value < 0.05, ***p-value < 0.001). Asterisks in parenthesis refer to p-values before Bonferroni–Hochberg correction (target genes populating the enriched ontologies are in Supplementary Data 2). (G, H) Heatmaps of raw reads from LHX2 ChIP-Seq peaks are plotted across nucleosome centered regions from age-matched ATAC-Seq samples. Each row represents a 3 kb window centered at maximum read pile-up. LHX2 motif occurrence in open chromatin regions is displayed and reported in Supplementary Tables 6. LHX2 motifs co-localize with RNA-Seq raw reads. Meta-profiles of the class II enhancer-associated H3K27ac marks were compiled at bidirectionally transcribed regions from the E14 (G) and P2 RPCs fractions (H) (background in gray, opposite strands replicates in hue). (I, J) Functional enrichment of Lhx2-dependent genes sets encoded within open chromatin regions (Supplementary Tables 6) by binomial distribution Figure provided by CiteAb. Source: Commun Biol, PMID: 31044167.



Flow Cytometry

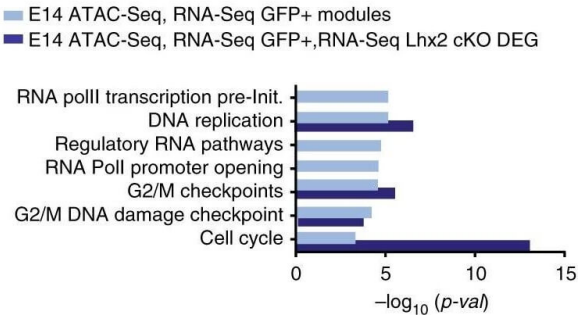
LHX2 coordinates variations in chromatin accessibility at the Sox2 locus. Custom tracks of E14 and P2 LHX2 ChIP-Seq reads and age-matched ATAC-Seq from purified RPCs and post mitotic precursors were configured on the mm10 UCSC murine genome assembly. Regions of interest targeted by LHX2, where variations by RNA-Seq and/or ATAC-Seq coverage are observed in Lhx2 cKO retinas are highlighted. Association with H3K27ac-labeled enhancer elements is also indicated. The LHX2-coordinated regulatory module is defined as follows: regulatory regions that display variations in ATAC-Seq coverage without a corresponding variation in the nearest transcript by E14 Lhx2 cKO RNA-Seq are putatively assigned (arrows) to the nearest gene exhibiting variation in transcript levels Figure provided by CiteAb. Source: Commun Biol, PMID: 31044167.



Flow Cytometry

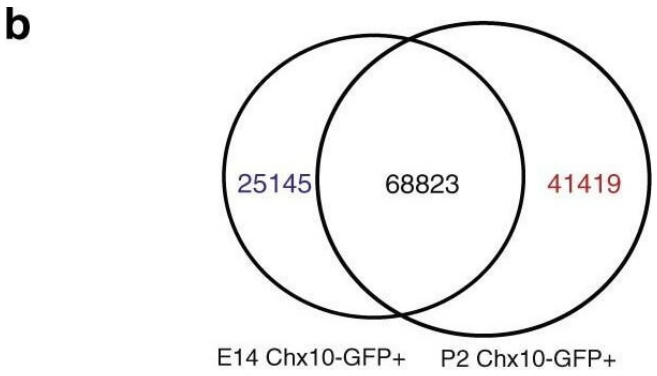
Binding sites for transcription factors with predicted pioneer function co-occur with LHX2 peaks. a, b Hierarchical clustering of LHX2 ChIP-Seq regulatory motifs and assigned representative logos are represented at E14 (a) and P2 (b) (linkage = average; similarity threshold cor = 0.6, ncor = 0.4, w = 5). The most enriched cluster comprises LHX2 and multiple variations of the same motif. (c, d) Known transcription factor motifs preferentially enriched in either E14 or P2 LHX2 ChIP-Seq peaks and identified by pairwise comparison are shown. Percentage of motif occurrences are reported for input and background datasets. The relative expression level of the corresponding transcription factor mRNA at E14/P2 is indicated by the blue/red color gradient, respectively Figure provided by CiteAb. Source: Commun Biol, PMID: 31044167.

i



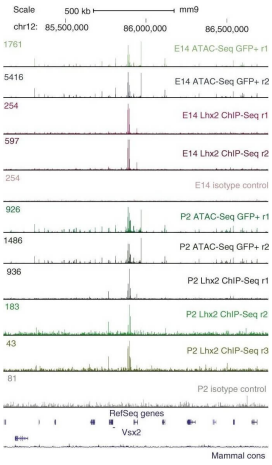
Flow Cytometry

LHX2 regulates cell cycle genes and the Notch signaling pathway by targeting promoters and non-coding elements in nucleosome free regions associated with active enhancers. a LHX2 motif density around the centers of ChIP-Seq peaks at E14 and P2. b Enrichment of LHX2 ChIP-Seq peaks distributed across different genomic regions (log2 fold enrichment). c–f Percentage of LHX2 target genes in retinal term assigned to at least one age-matched LHX2 ChIP-Seq peak. Enrichment was computed between target genes in term and total number of known genes in term (Supplementary Table 4 and Supplementary Data 1) for peaks shared at E14 and P2 (c), stage-specific peaks (d), and all peaks detected at E14 (e) and P2 (f). RNA-Seq from age-matched Lhx2 cKO retinas identifies Lhx2-dependent genes sets. (*p-value < 0.05, ***p-value < 0.001). Asterisks in parenthesis refer to p-values before Bonferroni–Hochberg correction (target genes populating the enriched ontologies are in Supplementary Data 2). g, h Heatmaps of raw reads from LHX2 ChIP-Seq peaks are plotted across nucleosome centered regions from age-matched ATAC-Seq samples. Each row represents a 3 kb window centered at maximum read pile-up. LHX2 motif occurrence in open chromatin regions is displayed and reported in Supplementary Tables 6. LHX2 motifs co-localize with RNA-Seq raw reads. Meta-profiles of the class II enhancer-associated H3K27ac marks were compiled at bidirectionally transcribed regions from the E14 (g) and P2 RPCs fractions (h) (background in gray, opposite strands replicates in hue). i, j Functional enrichment of Lhx2-dependent genes sets encoded within open chromatin regions (Supplementary Tables 6) by binomial distribution Figure provided by CiteAb. Source: Commun Biol, PMID: 31044167.



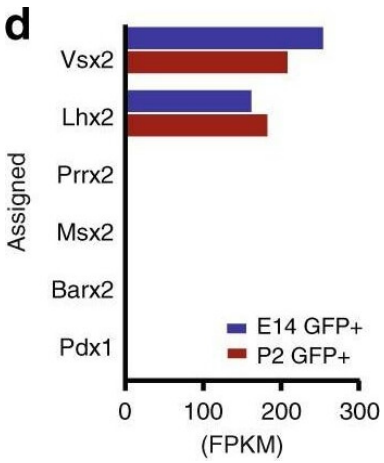
Flow Cytometry

Pairwise comparison of ATAC-Seq data identifies open chromatin regions from early and late RPCs, with a broad overrepresentation of LHX2 related motifs. A) Workflow for epigenomic profiling of RPC. B) Venn-diagram represents open chromatin regions identified in early- and late-stage VSX2 (CHX10)—GFP-positive RPCs. C) Hierarchical clustering of known motifs in the vertebrate genome (left, Jaspar 2016 non-redundant vertebrates core). Inset represents the major cluster of probabilistically assigned position weight matrices (PWMs) identified in open chromatin regions from early- and late-stage RPCs (scale = 1 node/pixel) (linkage = average; similarity threshold cor = 0.6, ncor = 0.4, w = 5) (Lhx2 instances as blue pixel strokes). D) Relative RNA-Seq expression for homeobox transcription factors. E) Representative LHX2 logos (MA0700.1, k-mer sig = 300, e-value = 1e-300), with positional variations of the same motif instance. F) Known motifs enrichment in open chromatin regions from early and late RPCs by binomial scoring of PWMs. G) LHX2 footprints from open chromatin regions identified in early- and late-stage RPCs. H) Custom tracks of RPC-derived ATAC-Seq profiles and aged-matched LHX2 ChIP-Seq feature the Vsx2 locus (mm9). Figure provided by CiteAb. Source: Commun Biol, PMID: 31044167.



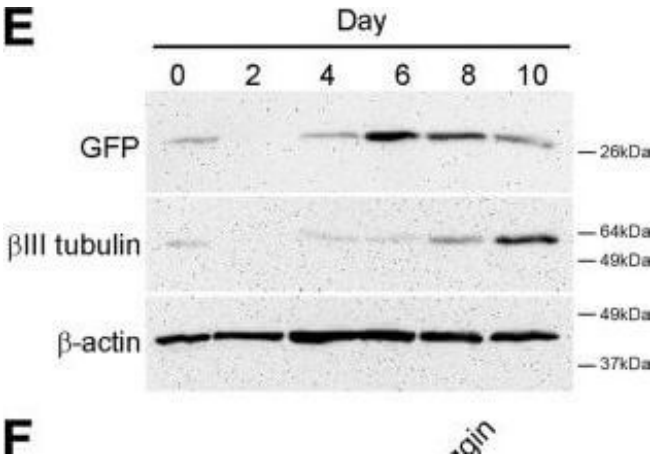
Flow Cytometry

Pairwise comparison of ATAC-Seq data identifies open chromatin regions from early and late RPCs, with a broad overrepresentation of LHX2 related motifs. A) Workflow for epigenomic profiling of RPC. B) Venn-diagram represents open chromatin regions identified in early- and late-stage VSX2 (CHX10)—GFP-positive RPCs. C) Hierarchical clustering of known motifs in the vertebrate genome (left, Jaspar 2016 non-redundant vertebrates core). Inset represents the major cluster of probabilistically assigned position weight matrices (PWMs) identified in open chromatin regions from early- and late-stage RPCs (scale = 1 node/pixel) (linkage = average; similarity threshold cor = 0.6, ncor = 0.4, w = 5) (Lhx2 instances as blue pixel strokes). D) Relative RNA-Seq expression for homeobox transcription factors. E) Representative LHX2 logos (MA0700.1, k-mer sig = 300, e-value = 1e-300), with positional variations of the same motif instance. F) Known motifs enrichment in open chromatin regions from early and late RPCs by binomial scoring of PWMs. G) LHX2 footprints from open chromatin regions identified in early- and late-stage RPCs. H) Custom tracks of RPC-derived ATAC-Seq profiles and aged-matched LHX2 ChIP-Seq feature the Vsx2 locus (mm9). Figure provided by CiteAb. Source: Commun Biol, PMID: 31044167.



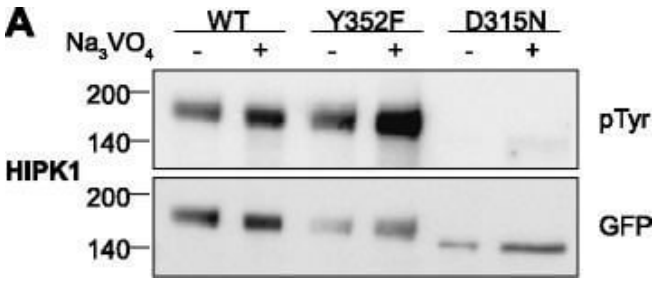
Flow Cytometry

Pairwise comparison of ATAC-Seq data identifies open chromatin regions from early and late RPCs, with a broad overrepresentation of LHX2 related motifs. A) Workflow for epigenomic profiling of RPC. B) Venn-diagram represents open chromatin regions identified in early- and late-stage VSX2 (CHX10)—GFP-positive RPCs. C) Hierarchical clustering of known motifs in the vertebrate genome (left, Jaspar 2016 non-redundant vertebrates core). Inset represents the major cluster of probabilistically assigned position weight matrices (PWMs) identified in open chromatin regions from early- and late-stage RPCs (scale = 1 node/pixel) (linkage = average; similarity threshold cor = 0.6, ncor = 0.4, w = 5) (Lhx2 instances as blue pixel strokes). D) Relative RNA-Seq expression for homeobox transcription factors. E) Representative LHX2 logos (MA0700.1, k-mer sig = 300, e-value = 1e-300), with positional variations of the same motif instance. F) Known motifs enrichment in open chromatin regions from early and late RPCs by binomial scoring of PWMs. G) LHX2 footprints from open chromatin regions identified in early- and late-stage RPCs. H) Custom tracks of RPC-derived ATAC-Seq profiles and aged-matched LHX2 ChIP-Seq feature the Vsx2 locus (mm9). Figure provided by CiteAb. Source: Commun Biol, PMID: 31044167.

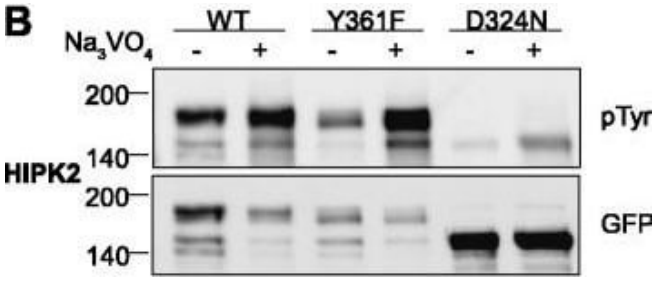


Western Blot

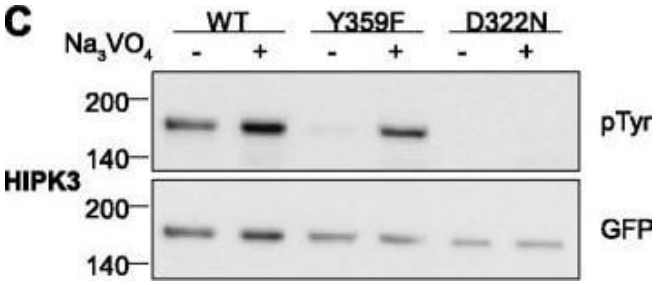
Npas4 expression during neural differentiation of ESCs. (A) RT-PCR analysis was used to determine the temporal expression profile of Npas4 mRNA in relation to various marker genes during N2B27 differentiation of mESCs (n = 3). Primers to the reference gene β-actin were used as a loading control. The negative control reaction (−) contained water in place of template cDNA. (B) The changes in Npas4 expression during N2B27 differentiation were quantified using qRT-PCR. At each time point Npas4 expression was normalized to β-actin expression and fold changes are relative to Day 0 (undifferentiated mESCs). Mean values and standard deviations of three independent experiments (n = 3) are displayed. (C)In situ hybridization analysis of Npas4 mRNA expression at Day 4 of N2B27 differentiation of mESCs. Representative images of differentiating colonies from two independent experiments (n = 2) are shown. Top panel - Npas4 antisense probe; Bottom panel - Npas4 sense probe. Scale bar = 100 µm. (D) Immunoblotting was used to determine the temporal expression profile of the Npas4 protein during N2B27 differentiation of mESCs. An antibody to the reference protein β-actin was used as a loading control (n = 3). (E) Immunoblotting was used to determine the temporal expression profile of Sox1 in the 46C cell line (using an antibody to GFP) and βIII tubulin during N2B27 differentiation of mESCs. An antibody to the reference protein β-actin was used as a loading control (n = 3). (F) RT-PCR analysis of NPAS4 mRNA in relation to various marker genes during Noggin-induced neural differentiation of hESCs (n = 3). Primers to the reference gene β-ACTIN were used as a loading control. The negative control reaction (−) contained water in place of template cDNA. hESCs, human embryonic stem cells; mESCs, mouse embryonic stem cells; NS, neurospheres. Figure provided by CiteAb. Source: Stem Cell Res Ther, PMID: 24887558.



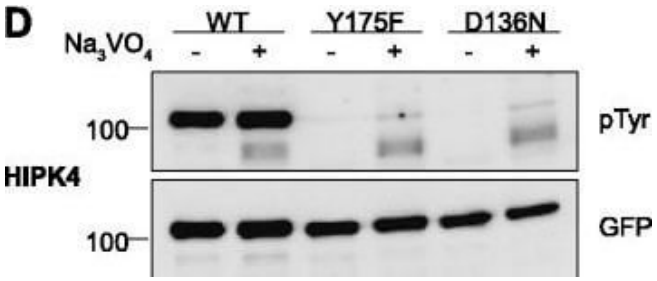
Western Blot
Tyrosine phosphorylation of HIPK mutants. HeLa cells were transiently transfected with the indicated expression constructs for HIPK1 (A), HIPK2 (B), HIPK3 (C) or HIPK4 (D). Sodium orthovanadate (Na3VO4) was added to every second sample for 1 h before lysis. GFP fusion proteins were immunoprecipitated and analysed by immunodetection with antibodies for pTyr and GFP. The panels are representative of 2–3 independent experiments. Figure provided by CiteAb. Source: Cell Commun Signal, PMID: 25630557.



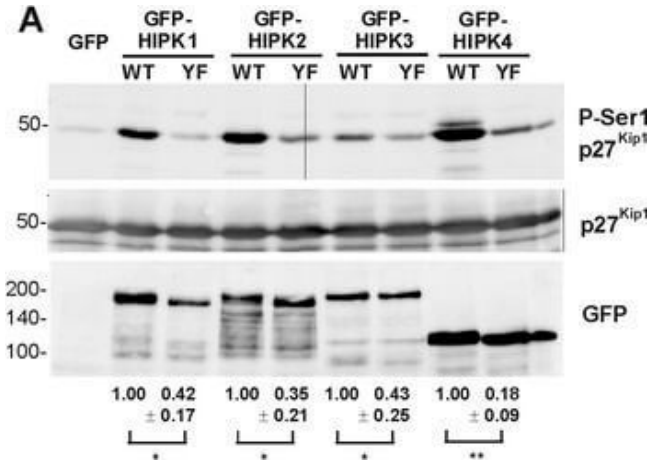
Western Blot
Tyrosine phosphorylation of HIPK mutants. HeLa cells were transiently transfected with the indicated expression constructs for HIPK1 (A), HIPK2 (B), HIPK3 (C) or HIPK4 (D). Sodium orthovanadate (Na3VO4) was added to every second sample for 1 h before lysis. GFP fusion proteins were immunoprecipitated and analysed by immunodetection with antibodies for pTyr and GFP. The panels are representative of 2–3 independent experiments. Figure provided by CiteAb. Source: Cell Commun Signal, PMID: 25630557.



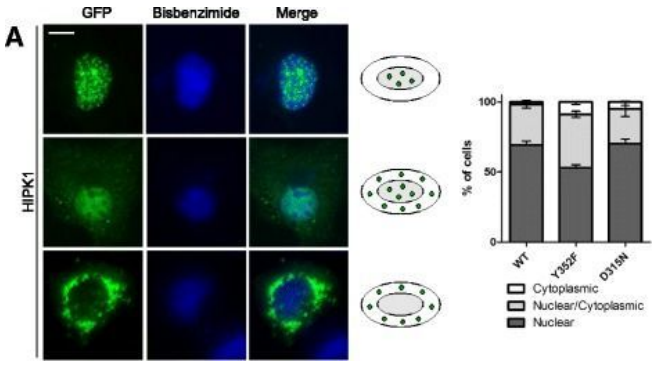
Western Blot
Tyrosine phosphorylation of HIPK mutants. HeLa cells were transiently transfected with the indicated expression constructs for HIPK1 (A), HIPK2 (B), HIPK3 (C) or HIPK4 (D). Sodium orthovanadate (Na3VO4) was added to every second sample for 1 h before lysis. GFP fusion proteins were immunoprecipitated and analysed by immunodetection with antibodies for pTyr and GFP. The panels are representative of 2–3 independent experiments. Figure provided by CiteAb. Source: Cell Commun Signal, PMID: 25630557.



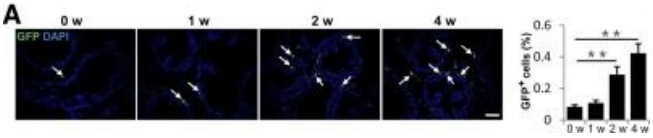
Western Blot
Tyrosine phosphorylation of HIPK mutants. HeLa cells were transiently transfected with the indicated expression constructs for HIPK1 (A), HIPK2 (B), HIPK3 (C) or HIPK4 (D). Sodium orthovanadate (Na3VO4) was added to every second sample for 1 h before lysis. GFP fusion proteins were immunoprecipitated and analysed by immunodetection with antibodies for pTyr and GFP. The panels are representative of 2–3 independent experiments. Figure provided by CiteAb. Source: Cell Commun Signal, PMID: 25630557.



Western Blot
Maximal activity of HIPKs depends on the activation loop tyrosine. Wild type GFP-HIPK fusion proteins and the respective Tyr→Phe mutants were immunoprecipitated from HeLa cells and subjected to kinase assays with recombinant GST-p27Kip1(A), myelin basic protein (B) or DYRKtide (C). GFP served as background control. A, Phosphorylation of p27Kip1 at Ser10 was detected by immunoblotting with a phosphorylation-specific antibody. For quantitative evaluation, pSer10 immunoreactivity was normalised to GFP immunoreactivity, which reflects the amount of kinase in the reaction. The blots illustrate a representative experiment, and the relative catalytic activities as determined from 3–4 assays are shown below the panels (means ± SD). One-sample t test: *, $p < 0.05$; **, $p < 0.01$. B and C, Phosphorylation of MBP and DYRKtide was measured in triplicate as incorporation of 32P. Background values from the GFP control samples were subtracted and activities were normalised to the amount of kinase in the reaction as determined by GFP immunoreactivity. Column diagrams illustrate catalytic activities relative to HIPK2 (WT). The results were replicated in independent experiments, except for a missing value of HIPK1. Figure provided by CiteAb. Source: Cell Commun Signal, PMID: 25630557.



Immunocytochemistry
Subcellular distribution of HIPK mutants. COS-7 cells were transfected with expression vectors for GFP-HIPK1 (A), GFP-HIPK2 (B), GFP-HIPK3 (C) or GFP-HIPK4 (D). The cellular localisation of the HIPK constructs was evaluated by imaging GFP autofluorescence in relation to bisbenzimide-stained nuclei. For each kinase, cells were classified into 3 major patterns that are illustrated by representative images and icons. The cells shown were transfected with (top to bottom) HIPK1 WT, DN, YF; HIPK2 WT, WT, YF; HIPK3 WT, WT, DN and HIPK4 DN, DN. A series of images of the different patterns for each kinase and its mutants is provided in the additional material (Additional file 1: Figure S3). Here the graphs show the percentages of cells classified into the indicated patterns (means ± SD, n = 3). In each of 3 experiments, at least 90 cells were evaluated for all HIPK constructs. Scale bars, 10 µm. Figure provided by CiteAb.
Source: Cell Commun Signal, PMID: 25630557.



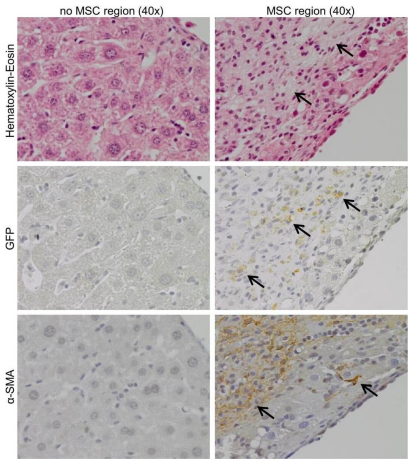
Immunohistochemistry

Increased nestin+ cells in prostate stroma are a subset of mesenchymal/stromal stem cells. (A): Immunofluorescence analysis of prostate tissue sections from Nestin-GFP transgenic mice at 0, 1, 2, and 4 weeks after initial PE injection using antibody against GFP. Arrows indicate GFP+ cells. Bar graph on the right shows the quantitative analyses of the ratio of GFP+ cells to total cells. Scale bar = 50μm. (B): Double-immunohistofluorescence analysis of prostate tissue sections from Nestin-GFP mice using antibodies against GFP and CD90 or Sca1. Scale bar = 20 μm. (C): Flow cytometry analysis of GFP+CD45–cells (percentage of total cells counted) in blood of Nestin-GFP mice at indicated time points after PE injection. (D): Flow cytometry analysis of CD90+Sca1+CD11b–CD45– cells (percentage of total cells counted) in blood of wild-type mice at indicated time points after PE injection. (E): Fluorescence-activated cell sorting of GFP+CD45−cells from ventral prostate tissue of 6-week-old Nestin-GFP mice. (F): Single CFU-F-derived GFP+CD45− cell strains were isolated and individually expanded for characterization assays. (G): Single GFP+CD45− clones were isolated, expanded, and cultured. Cells were separately incubated with fibrogenic media, osteogenic media, adipogenic media, and chondrogenic media, and they were stained for vimentin (upper left panel), Alizarin Red S (upper right panel), Oil Red O (lower left panel), and Toluidine Blue (lower right panel), respectively. (H): Double-immunohistofluorescence analysis of prostate tissue sections from 6-week-old Nestin-Cre, Rosa26-YFPflox/+ mice using antibodies against YFP (green) and vimentin (red, top panels) or α-SMA (red, bottom panels). Scale bar = 50μm. n = 4–5 per group. Data are shown as the mean ± SD. □, $p < .05$, □□, $p < .01$ determined by multifactorial analysis of variance. Abbreviations: CFU-F, colony-forming unit fibroblast; DAPI, 4’,6-diamidino-2-phenylindole; GFP, green fluorescent protein; PE, phenylephrine; α-SMA, α-smooth muscle actin; w, weeks. Figure provided by CiteAb. Source: Stem Cells Transl Med, PMID: 28191756.

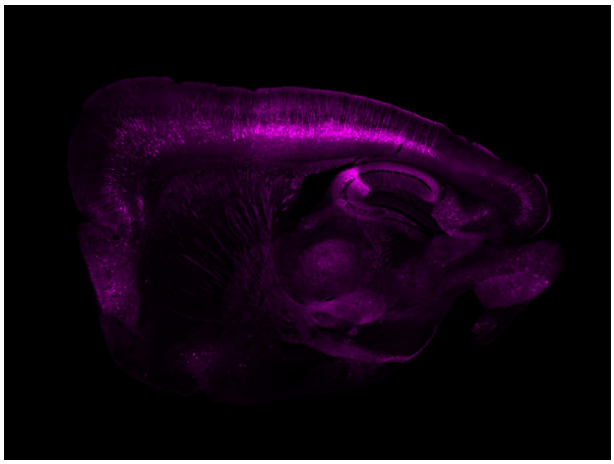


Immunohistochemistry

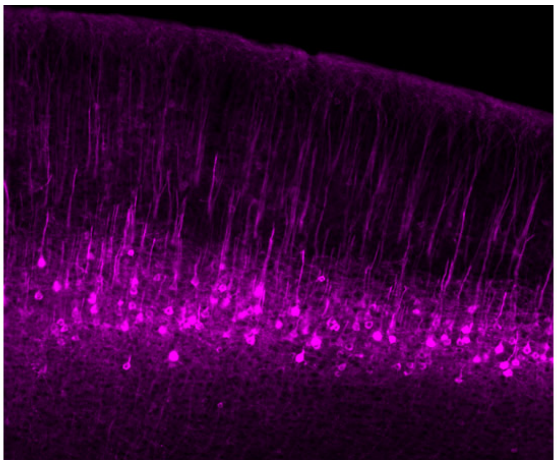
Increased nestin+ cells in prostate stroma are a subset of mesenchymal/stromal stem cells. (A): Immunofluorescence analysis of prostate tissue sections from Nestin-GFP transgenic mice at 0, 1, 2, and 4 weeks after initial PE injection using antibody against GFP. Arrows indicate GFP+ cells. Bar graph on the right shows the quantitative analyses of the ratio of GFP+ cells to total cells. Scale bar = 50µm. (B): Double-immunohistofluorescence analysis of prostate tissue sections from Nestin-GFP mice using antibodies against GFP and CD90 or Sca1. Scale bar = 20 µm. (C): Flow cytometry analysis of GFP+CD45–cells (percentage of total cells counted) in blood of Nestin-GFP mice at indicated time points after PE injection. (D): Flow cytometry analysis of CD90+Sca1+CD11b–CD45– cells (percentage of total cells counted) in blood of wild-type mice at indicated time points after PE injection. (E): Fluorescence-activated cell sorting of GFP+CD45−cells from ventral prostate tissue of 6-week-old Nestin-GFP mice. (F): Single CFU-F-derived GFP+CD45− cell strains were isolated and individually expanded for characterization assays. (G): Single GFP+CD45− clones were isolated, expanded, and cultured. Cells were separately incubated with fibrogenic media, osteogenic media, adipogenic media, and chondrogenic media, and they were stained for vimentin (upper left panel), Alizarin Red S (upper right panel), Oil Red O (lower left panel), and Toluidine Blue (lower right panel), respectively. (H): Double-immunohistofluorescence analysis of prostate tissue sections from 6-week-old Nestin-Cre, Rosa26-YFPflox/+ mice using antibodies against YFP (green) and vimentin (red, top panels) or α-SMA (red, bottom panels). Scale bar = 50µm. n = 4–5 per group. Data are shown as the mean ± SD. ⍰, $p < .05$, ⍰⍰, $p < .01$ determined by multifactorial analysis of variance. Abbreviations: CFU-F, colony-forming unit fibroblast; DAPI, 4’,6-diamidino-2-phenylindole; GFP, green fluorescent protein; PE, phenylephrine; α-SMA, α-smooth muscle actin; w, weeks. Figure provided by CiteAb. Source: Stem Cells Transl Med, PMID: 28191756.



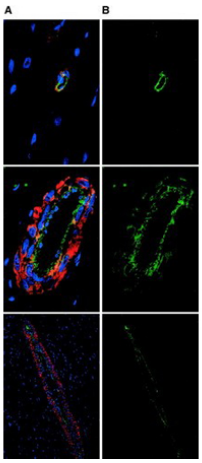
Immunohistochemistry
MSCs are traced in special organized regions. MSC regions and normal regions in regenerated liver tissue of cirrhotic mice treated with pHx + 2 x 106 MSC stained for Haematoxylin-eosin, GFP and α-SMA (40x magnifications, MSCs are indicated by the black arrows). GFP, green fluorescent protein; α-SMA, smooth muscle actin; MSCs, mesenchymal stromal cells; pHx, partial hepatectomy Figure provided by CiteAb. Source: J Cell Mol Med, PMID: 31245923.



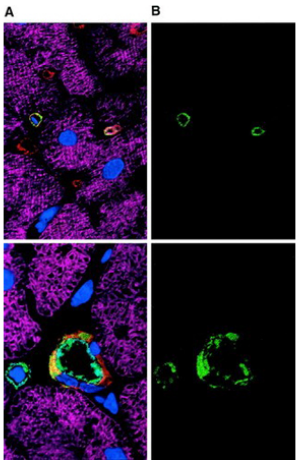
Immunofluorescence Microscopy
Immunofluorescence results using Goat Anti-GFP Antibody. Staining was performed on free-floating 40µm mouse brain sections. Heat antigen retrieval was performed for 30 minutes at 80°C in sodium citrate buffer (pH 8.9). Sections were blocked in 5% donkey serum with 0.25% Triton X-100 for 1h at RT, then incubated overnight at 4°C in a 1:1000 dilution of Goat Anti-GFP (p/n 600-101-215). Sections were then washed and incubated for 2h at RT in a 4µg/mL solution of donkey anti-rabbit AF647-conjugated secondary antibody. 10X fluorescence images were obtained using a Zeiss Axioscan automated slide scanning microscope. Low mag. Image courtesy of Michael Castle lab, University of California, San Diego.



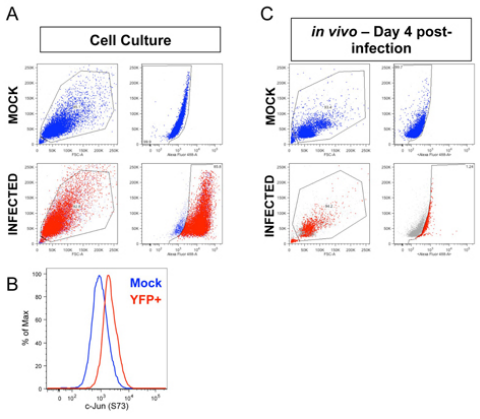
Immunofluorescence Microscopy
Immunofluorescence results using Goat Anti-GFP Antibody. Staining was performed on free-floating 40µm mouse brain sections. Heat antigen retrieval was performed for 30 minutes at 80°C in sodium citrate buffer (pH 8.9). Sections were blocked in 5% donkey serum with 0.25% Triton X-100 for 1h at RT, then incubated overnight at 4°C in a 1:1000 dilution of Goat Anti-GFP (p/n 600-101-215). Sections were then washed and incubated for 2h at RT in a 4µg/mL solution of donkey anti-rabbit AF647-conjugated secondary antibody. 10X fluorescence images were obtained using a Zeiss Axioscan automated slide scanning microscope. High mag. Image courtesy of Michael Castle lab, University of California, San Diego.



Immunofluorescence Microscopy
Confocal microscopy of left ventricular (LV) free wall tissue sections. Tissues were stained with anti-green fluorescent protein (GFP) antibody (green), anti α-smooth muscle actin (red) to identify smooth muscle cells, and propidium iodide (blue) to identify nuclei (A). A: nuclei of several nonsmooth muscle cells (i.e., cardiomyocytes), which did not stain with anti-GFP antibody. B: spontaneous green fluorescence is shown alone. Green fluorescence of GFP is demonstrated in endothelial and smooth muscle cells of small and large arterioles and also in the adventitial layer of the large arteriole (B). Fig 1.
PMID: 12844500

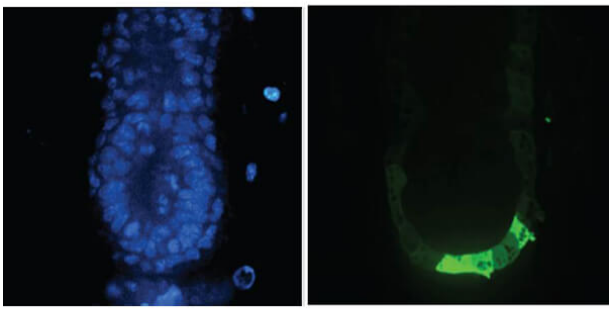


Immunofluorescence Microscopy
Confocal microscopy of LV free wall tissue sections. Of 8 capillaries, identified by anti-human von Willebrand factor (vWF) (endothelial cells, red), two are positive for GFP (A, top). A, bottom: a capillary and an arteriole are positive for using the antibody to GFP. Myocytes (purple), nuclei (dark blue), endothelial cells (light blue), and smooth muscle cells (red) are shown. B: antibody staining for GFP confirms GFP expression (green) in vascular structures. Fig 2.
PMID: 12844500



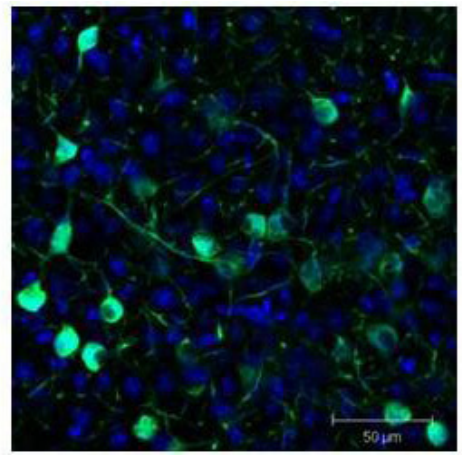
Flow Cytometry

Enhanced c-Jun S73 phosphorylation occurs specifically in infected cells. (A and B) 3T3 fibroblasts were mock-infected or infected with H2B-YFP-expressing MHV68 (Collins and Speck, 2012) at MOI = 5 PFU/cell. 18 h post-infection cells were harvested and processed for intracellular antigen staining to detect H2B-YFP (A) or c-Jun phosophorylated on S73 (B) by flow cytometry. H2B-YFP expressing cells were identified by flow cytometry following staining with goat anti-GFP (Rockland Immunochemicals) and donkey anti-goat Alexa 488 (Invitrogen). H2B-YFP+ cells were identified relative to mock-infected cells. c-Jun (S73) intensities were determined in mock-infected and H2B-YFP+ cells by flow cytometry following staining with PE-conjugated rabbit anti-phospho-S73 c-Jun (Cell Signaling Technology). Isotype controls were used to determine background staining intensity (not shown). (C) 6–8 week-old C57BL/6 mice were intraperitoneally mock-inoculated or inoculated with 106 PFU of H2B-YFP-expressing MHV68. 4 days post-infection, mice were sacrificed, and splenocytes were isolated and processed as in A and B to detect H2B-YFP and S73-phosphorylated c-Jun (See Figure 3). Shown are representative dot plots to demonstrate the relative percentage of H2B-YFP+ cells detected in infected animals and the gating strategy used to segregate YFP− and YFP+ cells for comparative analyses of c-Jun phosphorylation within the same animal. A total of 3 mock-inoculated and 4 H2B-YFP MHV68 inoculated animals were used for these experiments. Figure S3. PMID: 24068923



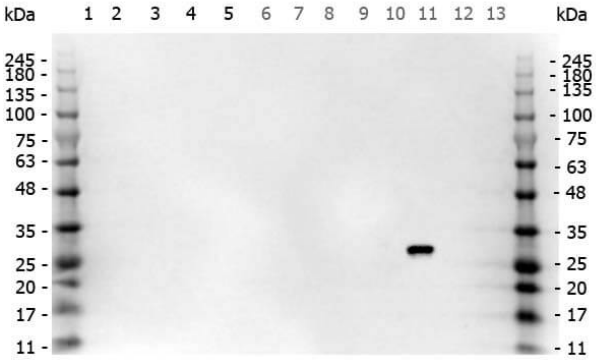
Immunofluorescence Microscopy

Immunofluorescence Microscopy of Anti-GFP (GOAT) Antibody. Tissue: E5.5 Hex-GFP transgenic mouse embryo. Primary antibody: Goat anti-GFP was used at 1:500 dilution. Secondary antibody: Fluorchrome conjugated Anti-goat IgG secondary antibody at 1:10,000 for 45 min at RT. Staining: GFP as green fluorescent signal with DAPI blue counterstain.



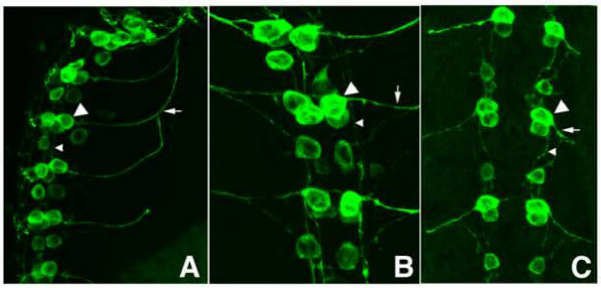
Immunofluorescence Microscopy

Immunofluorescence Microscopy of Goat Anti-GFP Antibody. Tissue: Sf-1:Cre mice crossed to the Z/EG reporter line. Mouse brain (coronal view, 20X magnification). Fixation: 4%PFA/PBS with o/n fixation, and subsequently transferred to a 30% sucrose solution. Antigen retrieval: frozen in OCT freezing medium (Sakura) and cryostat sectioned at 40 microns. Primary antibody: Goat anti-GFP was used at 1:500 dilution in free floating immunohistochemistry to detect GFP. Secondary antibody: Fluorochrome conjugated Anti-goat IgG secondary antibody was used for detection at 1:500 at 1:10,000 for 45 min at RT. Localization: Sf-1+ neurons and their processes of the ventromedial nucleus of the hypothalamus. Staining: eGFP as green fluorescent signal and sections were counterstained with DAPI.

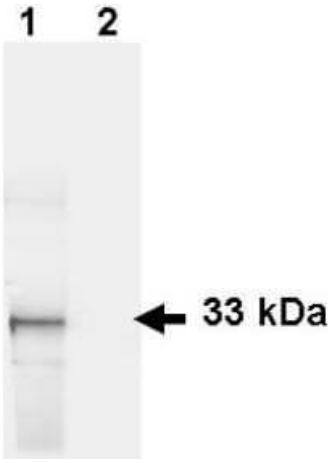


Western Blot

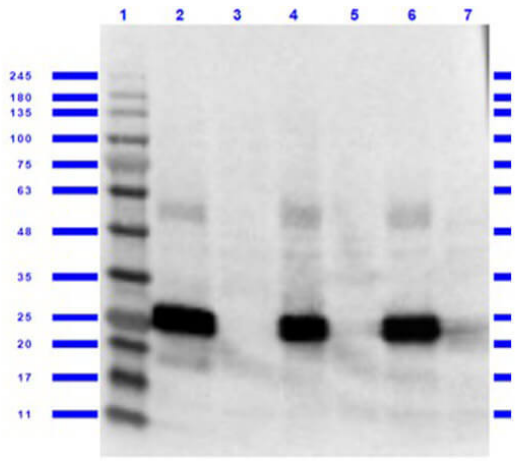
Multi-lysate Western Blot of Goat anti-GFP antibody. Marker: Opal Pre-stained ladder (p/n MB-210-0500). Lane 1: HEK293 lysate (p/n W09-000-365). Lane 2: HeLa Lysate (p/n W09-000-364). Lane 3: CHO/K1 Lysate (p/n W07-000-357). Lane 4: MDA-MB-231 (p/n W09-001-GK6). Lane 5: A431 Lysate (p/n W09-000-361). Lane 6: Jurkat Lysate (p/n W09-001-370). Lane 7: NIH/3T3 Lysate (p/n W10-000-358). Lane 8: E-coli HCP Control (p/n 000-001-J08). Lane 9: FLAG Positive Control Lysate (p/n W00-001-383). Lane 10: Red Fluorescent Protein (p/n 000-001-379). Lane 11: Green Fluorescent Protein (p/n 000-001-215). Lane 12: Glutathione-S-Transferase Protein (p/n 000-001-200). Lane 13: Maltose Binding Protein (p/n 000-001-385). Load: 10 µg of lysate or 50ng of purified protein per lane. Primary antibody: GFP antibody at 1ug/mL overnight at 4C. Secondary antibody: Peroxidase goat secondary antibody at 1:30,000 for 60 min at RT. Blocking Buffer: 1% Casein-TTBS (p/n MB-082) for 30 min at RT. Predicted/Observed size: 30 kDa for GFP.



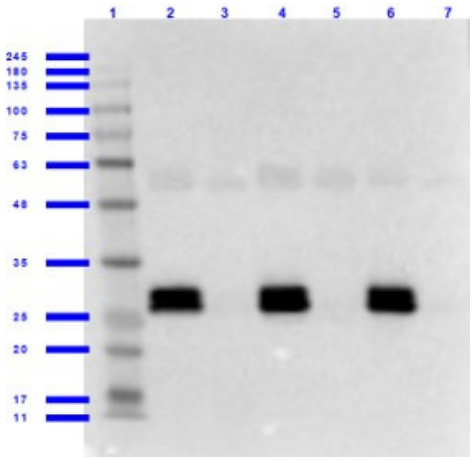
Immunofluorescence Microscopy
Immunofluorescence Microscopy of GFP-GOAT Antibody. Tissue: Drosophila melanogaster late stage embryonic central nervous system. Fixation: 0.5% PFA. Antigen retrieval: not required. Primary antibody: Anti-GFP antibody at a 1:1,000 for 1 h at RT. Secondary antibody: AlexaFluor 488™ conjugated Anti-Goat antibody at 1:300 for 45 min at RT. Panel A: shows a lateral view (ventral left). Panels B and C: shows ventral views of whole mount embryos at 63x magnification (plus 2x digital zoom). In all panels, anterior is up. Staining: tau-GFP cell bodies (large arrowhead) and axons of motorneurons (arrow) and interneurons (small arrowhead) as green fluorescent signal.



Western Blot
Western Blot of Goat anti-GFP antibody. Lane 1: HeLa cells. Lane 2: mock transfected HeLa cell lysate. Load: 35 µg per lane. Primary antibody: GFP antibody at 1 µg/ml for 1 h at room temperature. Secondary antibody: IRDye® 800 conjugated Donkey-a-Goat IgG [H&L] MX7 (605-732-125) secondary antibody at 1:2,500 for 45 min at RT. Block: 5% BLOTTO overnight at 4°C. Predicted/Observed size: 27 kDa, 33 kDa for GFP. Other band(s): none.



Western Blot
Western Blot of Goat anti-GFP antibody with lysates. Lane 1: Opal Prestained Molecular Weight Marker (p/n MB-210-0500). Lane 2: GFP/HEK293T WCL (p/n 000-001-215/W09-001-GX5) [0.05/10µg]. Lane 3: HEK293T WCL (p/n W09-001-GX5) [10µg]. Lane 4: GFP/NIH-3T3 WCL (p/n 000-001-215/W10-000-358) [0.05/10µg]. Lane 5: NIH-3T3 WCL (p/n W10-000-358) [10µg]. Lane 6: GFP/PC-12 WCL (p/n 000-001 -215/W12-001-GL9) [0.05/10µg]. Lane 7: PC-12 WCL (p/n W12-001-GL9) [10µg]. Primary antibody: Anti-GFP antibody at 1ug/mL overnight at 2-8°C. Secondary antibody: Donkey Anti-Goat IgG HRP secondary antibody (p/n 605-703-002) at 1:40,000 for 30 min at RT. Blocking Buffer: BlockOut Buffer (p/n MB-073) for 1hr at RT. Predicted/Observed size: ~27kDa for GFP.



Western Blot
Western Blot of Goat anti-GFP Antibody with Serums. Lane 1: Opal Prestained Molecular Weight Marker (p/n MB-210-0500). Lane 2: GFP/Human Serum (p/n 000-001-215/D314-05) [0.01/0.02µL] [+]. Lane 3: Human Serum (p/n D314-05) [0.02µL] [-]. Lane 4: GFP/Mouse Serum (p/n 000-001-215/D308-05) [0.01/0.02µL] [+]. Lane 5: Mouse Serum (p/n D308-05) [0.02µL] [-]. Lane 6: GFP/Rat Serum (p/n 000-001-215/D310-05) [0.01/0.02µL] [+]. Lane 7: Rat Serum (p/n D310-05) [0.02µL] [-]. Primary antibody: Anti-GFP antibody at 1.0ug/mL overnight at 2-8°C. Secondary antibody: Donkey Anti-Goat IgG HRP secondary antibody (p/n CUSTmx8) at 1:40,000 for 30 min at RT. Blocking Buffer: BlockOut Buffer (p/n MB-073) for 1hr at RT. Predicted/Observed size: ~27kDa for GFP.

References

- Urrutia HA et al. Placode-derived orphan chemokine CXCL14 is critical for proper chick trigeminal ganglion formation. *Dev Biol.* (2026)
- Newbold SA et al. The intracellular domain of the epilepsy protein PCDH19 regulates spine density in cortical neurons in vivo via Xlr genes. *J Neurosci.* (2026)
- Li SJ et al. A disinhibitory basal forebrain-to-cortex projection supports sustained attention. *Cell.* (2026)
- Xiao W et al. Peri-head distance coding in the mouse brainstem. *Neuron.* (2026)
- Tu R et al. The E-cadherin-Wnt-mir-994 Axis Repurposes a Cadherin Switch for Niche Robustness and Germline Stem Cell Maintenance. *Cell Prolif.* (2026)
- Kondoh K et al. Nos1 neurons in the paraventricular hypothalamic area modulate lipid metabolism via the sympathetic nervous system in male mice. *Nat Commun.* (2026)
- Lewy T et al. Brain endothelial cells orchestrate a neuroprotective antiviral state in the CNS in response to peripheral viral pattern sensing. *Immunity.* (2026)
- Wang D et al. A universal 6iL/E4 culture system for deriving and maintaining embryonic stem cells across mammalian species. *Cell Res.* (2026)
- Ibrahimi M et al. TRACR: an anterograde transneuronal tracing system for genetic access across synapses and longitudinal circuit analysis. *bioRxiv [Preprint].* (2026)
- Chiu YT et al. A suite of engineered mice for interrogating psychedelic drug actions. *Nat Neurosci.* (2026)
- Assir MZ et al. Modeling maternal immune activation in 3D ex vivo human fetal brain cerebroids reveals IL-17A-driven disruption of cortical development. *Nat Neurosci.* (2026)
- Fisher JD et al. Convergent olfactory circuits for courtship in Drosophila revealed by the circuit-tracing tool ds-Tango. *Curr Biol.* (2026)

- Isaji T et al. ST3GAL3-mediated selective α2, 3-sialylation of LDLR promotes vesicular stomatitis virus entry. *Biochim Biophys Acta Gen Subj.* (2026)
- Fiske BE et al. Lyn governs the establishment and maintenance of B cell anergy by suppressing PI3K signaling. *Nat Commun.* (2026)
- Barnes DT et al. Delta family protocadherins contribute to protoglomerular targeting of olfactory sensory neuron axons in the olfactory bulb. *PLoS Genet.* (2026)
- Liu Z et al. Identification of a potential internalization or endocytic compartment-targeting signal in the C-terminal tail of the tetraspanin protein TSP-12. *MicroPubl Biol.* (2026)
- Fordyce BA et al. No evidence for direct physical interaction of 5-HT2A-mGluR2 receptors in vitro or in vivo. *bioRxiv [Preprint].* (2026)
- Botts SR et al. ERG preserves endothelial identity to limit atherosclerosis. *Nat Commun.* (2026)
- Viola C et al. Activation of GCaMP6f-Expressing Chromaffin and Satellite Glial Cells in Murine Adrenal Slices by Nanosecond Electric Pulses. *J Neurochem.* (2026)
- Bussaka K et al. Barrington's Nucleus: A Pontine Defecation Brain Area Exhibiting Prompt and Delayed Defecation Responses. *Cell Mol Gastroenterol Hepatol.* (2026)
- Jung H et al. Autism-associated ARHGEF9 variants impair GABAergic synapses and ultrasonic communication by reducing gephyrin phosphorylation. *Mol Psychiatry.* (2026)
- Bao H et al. Aberrantly integrated adult-born immature neurons disrupt brain-wide networks during spatial memory processing. *Mol Psychiatry.* (2026)
- Belfi AC et al. Opposing roles for lipocalins and a CD36 family scavenger receptor in apical extracellular matrix-dependent protection of narrow tube integrity. *Development.* (2026)
- Procacci NM et al. GCaMP6f-expressing chromaffin cells in murine adrenal slices exhibit dynamic spontaneous calcium responses that do not require nerve input. *Cell Calcium.* (2026)
- Savas D et al. Feeding decision-making by a single neuron via disparate neurotransmitters. *Nat Commun.* (2026)
- Hu Y et al. Degradation of LOX-1 via Neuronal Autophagy Alleviates Cerebral Ischemia/Reperfusion Injury in Mice. *Mol Neurobiol.* (2026)
- Liu K et al. The AAA-ATPase Yta4 inhibits the interaction between Ppa2 and Atg43 to promote Atg43 phosphorylation and mitophagy. *J Biol Chem.* (2026)
- Bohlen MO et al. Projection targeting with phototagging to study the structure and function of retinal ganglion cells. *Cell Rep Methods.* (2026)
- Osório C et al. Purkinje cell intrinsic activity shapes cerebellar development and function. *Nat Commun.* (2026)
- Kim S et al. Bazedoxifene reverses sexually dimorphic autistic-like abnormalities in biallelic MDGA1-mutant mice. *EMBO Mol Med.* (2026)
- Ibrahim KE et al. In vivo CAR T cell generation using retargeted and functionalized lentiviral vectors with reduced immunogenicity. *Nat Commun.* (2026)
- Zheng S et al. The endoplasmic reticulum protein Erg28 restrains Mto1-Mto2-γ-TuSC-mediated microtubule assembly. *Cell Rep.* (2026)

- Kankanamge LP et al. Nrf1 coordinates proteasome activity and autophagy to maintain cardiac proteostasis. *Commun Biol.* (2026)
- Świst-Rosowska KM et al. The basic domain of Suv39h2 buffers mitoxantrone-induced heterochromatin destabilization. *iScience.* (2026)
- Godschall EN et al. A brain reward circuit inhibited by next-generation weight-loss drugs in mice. *Nature.* (2026)
- Yu X et al. Retrograde optogenetics reveals sensorimotor convergence within a corticotectal pathway of non-human primates. *Curr Biol.* (2026)
- Ibrahimi, M et al. TRACR: an anterograde transneuronal tracing system for genetic access across synapses and longitudinal circuit analysis. *BioRxiv [Preprint]* (2026)
- Wu Y et al. Multimodal transcriptomics reveal neurogenic aging trajectories and age-related regional inflammation in the dentate gyrus. *Nat Neurosci.* (2025)
- Belfi AC et al. Opposing roles for lipocalins and a CD36 family scavenger receptor in apical extracellular matrix-dependent protection of narrow tube integrity. *bioRxiv [preprint]* (2025)
- Cadeddu R et al. Prefrontal 5α-reductase 2 mediates male-specific acute stress response. *Sci Adv.* (2025)
- Buss EW et al. Regulation by Presynaptic NMDA Receptors of Non-Linear Postsynaptic Summation of the Cortical Input to CA1 Pyramidal Neurons. *Neuroscience.* (2025)
- Ahmad S et al. Small Extracellular Vesicles Promote Axon Outgrowth by Engaging the Wnt-Planar Cell Polarity Pathway. *Cells.* (2025)
- Oñate MK et al. Stromal KITL/SCF Maintains Pancreas Tissue Homeostasis and Restrains Tumor Progression. *Cancer Discov.* (2025)
- Thakur P et al. An antisense oligonucleotide-based strategy to ameliorate cognitive dysfunction in the 22q11.2 Deletion Syndrome. *Elife.* (2025)
- Cassidy RM et al. Complementary Organization of Mouse Driver and Modulator Cortico-thalamo-cortical Circuits. *J Neurosci.* (2025)
- Jiang Y et al. Effects of chromosome number reduction on mitotic and meiotic stability in fission yeast. *Genome Biol.* (2025)
- Owens SM et al. Intrinsic p53 activation restricts gammaherpesvirus driven germinal center B cell expansion during latency establishment. *Nat Commun.* (2025)
- Kam Yan Kwok R et al. Validation of phiC31-mediated expression and functional knockout of Opn3 in the Opn3-phiC31o knock-in mouse. *Eye Vis (Lond).* (2025)
- Li X et al. Examining the role of Notch signaling in dysplastic lung repair. *BMC Res Notes.* (2025)
- View More ...

Disclaimer

This product is for research use only and is not intended for therapeutic or diagnostic applications. Please contact a technical service representative for more information. All products of animal origin manufactured by Rockland Immunochemicals are derived from starting materials of North American origin. Collection was performed in United States Department of Agriculture (USDA) inspected facilities and all materials have been inspected and certified to be free of disease and suitable for exportation. All properties listed are typical characteristics and are not specifications. All suggestions and data are offered in good faith but without guarantee as conditions and methods of use of our products are beyond our control. All claims must be made within 30 days following the date of delivery. The prospective user must determine the suitability of our materials before adopting them on a commercial scale. Suggested uses of our products are not recommendations to use our products in violation of any patent or as a license under any patent of Rockland Immunochemicals, Inc. If you require a commercial license to use this material and do not have one, then return this material, unopened to: Rockland Inc., P.O. BOX 5199, Limerick, Pennsylvania, USA.